

RECONSTRUCTION OF THE 2D HOLE GAS SPECTRUM FOR SELECTIVELY DOPED p -Ge/Ge_{1-x}Si_x HETEROSTRUCTURES

*Yu. G. Arapov, G. I. Harus, V. N. Neverov, N. G. Shelushinina, M. V. Yakunin**

*Institute of Metal Physics RAS
GSP-170, 620219, Ekaterinburg, Russia*

O. A. Kuznetsov

Scientific-Research Institute at Nizhnii Novgorod State University, Russia

Submitted 22 July 2002

The magnetic field ($0 \leq B \leq 32$ T) and temperature ($0.1 \leq T \leq 15$ K) dependences of longitudinal and Hall resistivities have been investigated for p -Ge_{0.93}Si_{0.07}/Ge multilayers with different Ge layer widths $12 \text{ nm} \leq d_w \leq 20 \text{ nm}$ and hole densities $p_s = (1-5) \cdot 10^{15} \text{ m}^{-2}$. An extremely high sensitivity of the experimental data (the structure of magnetoresistance traces, relative values of the inter-Landau-level gaps deduced from the activation magnetotransport, etc.) to the quantum well profile is revealed in the cases where the Fermi level reaches the second confinement subband. An unusually high density of localized states between the Landau levels is deduced from the data. Two models for the long-range random impurity potential (the model with randomly distributed charged centers located outside the conducting layer and the model of the system with a spacer) are used to evaluate the impurity potential fluctuation characteristics: the random potential amplitude, the nonlinear screening length in the vicinity of integer filling factors $\nu = 1$ and $\nu = 2$, and the background density of states (DOS). The described models are suitable for explanation of the observed DOS values, while the short-range impurity potential models fail. For half-integer filling factors, the linear temperature dependence of the effective quantum Hall effect plateau-plateau (PP) transition widths $\nu_0(T)$ is observed, contrary to the expected scaling behavior of the systems with short-range disorder. The finite $T \rightarrow 0$ width of the PP transitions may be due to an effective low-temperature screening of a smooth random potential due to the Coulomb repulsion of electrons.

PACS: 73.43.-f

1. INTRODUCTION

The p -type modulation-doped heterostructures on the basis of Si, Ge, and their alloys are of interest in device physics, in view of Si-based chip technology for fabrication of high-performance transistors, intra-chip optical interconnects, and possible applications in fiber-optic telecommunications. Many quantum physical aspects could be foreseen in investigations of this heterosystem because of specific features of the valence band structure, which might be varied dramatically by the extent of the hole confinement and uniaxial stress arising from the lattice mismatch. Because the band offset in the Ge-Si heterosystem is almost entirely located in the valence band, the confinement of electrons

is hardly achievable and 2D conductance is mainly due to holes.

Until presently, the research has mostly been performed on the Si-side compounds, like the Si/Si_{1-x}Ge_x/Si quantum well (QW), to be best compatible with the Si substrate [1]. In this case, the hole conductivity is via the Si-Ge alloy. In this paper, we present the results obtained on a high-quality two-dimensional hole gas (2DHG) realized in the heterosystems on the Ge side, in the p -Ge_{1-x}Si_x/Ge heterostructures with a small amount of Si. In this case, the 2DHG is confined not in an alloy with randomly distributed Ge and Si atoms within the crystal lattice, but in a uniform Ge crystal layer, which works towards a decrease of the number of imperfections [2].

Much knowledge on the valence band properties

*E-mail: yakunin@imp.uran.ru

can be obtained under conditions of its magnetic field quantization, especially in the case where it is spatially quantized in addition. Some information on the intricate Landau level (LL) structure of the valence band can be obtained from the quantum cyclotron resonance [2, 3]. This experiment yields distances between the adjacent levels positioned in each series on the opposite sides of the Fermi level. Similar probing of the LL diagram within its cut by the Fermi level can be realized by means of the activation magnetotransport analysis under the quantum Hall regime. Distances between the adjacent LLs are then extracted irrespective of their classification in certain series because there are no restrictions due to optical selection rules. Moreover, a detailed scrutiny of the states distributed between the adjacent LLs can be achieved from scanning them by the Fermi level in experiments of this kind.

The analysis of temperature dependence of the Hall and longitudinal magnetoresistivity both in the plateau and in the plateau–plateau transition regions allows extracting such electron spectrum parameters as the energy separation between adjacent LLs, the relative fractions of localized and extended states, the density of localized states, and the width of extended state bands. Experimental reconstruction of the energy spectrum is specially important for *p*-type systems with a complex valence band spectrum, in which the LL picture is not determined by only the cyclotron energy with a given effective mass as for the *n*-type system with a simple parabolic conduction band.

2. EXPERIMENTAL TECHNIQUE

A series of multilayered $p\text{-Ge}_{1-x}\text{Si}_x/\text{Ge}$ ($x \approx 0.07$) heterostructures differing in the Ge layer width in the range $d_w = 12\text{--}20$ nm and the hole density per single Ge layer $p_s = (1\text{--}5) \cdot 10^{15} \text{ m}^{-2}$ were grown by hydride vapor deposition on the Ge(111) substrate. The undoped Ge buffer was grown first, followed by the undoped $\text{Ge}_{1-y}\text{Si}_y$ buffer and then by several undoped $\text{Ge}_{1-x}\text{Si}_x/\text{Ge}$ periods and a certain number of periods with $\text{Ge}_{1-x}\text{Si}_x$ barriers doped symmetrically with boron in their central parts (having undoped spacers about 1/4 the barrier width on both sides of the barriers): see the inset in Fig. 2 below. The relation between the Si content in the buffer (y) and in the multilayers (x) predetermines the distribution of mismatch stress between the Ge and $\text{Ge}_{1-x}\text{Si}_x$ layers. The barriers are sufficiently wide to avoid the inter-Ge-layer tunneling. The low-temperature hole mobilities are in the range

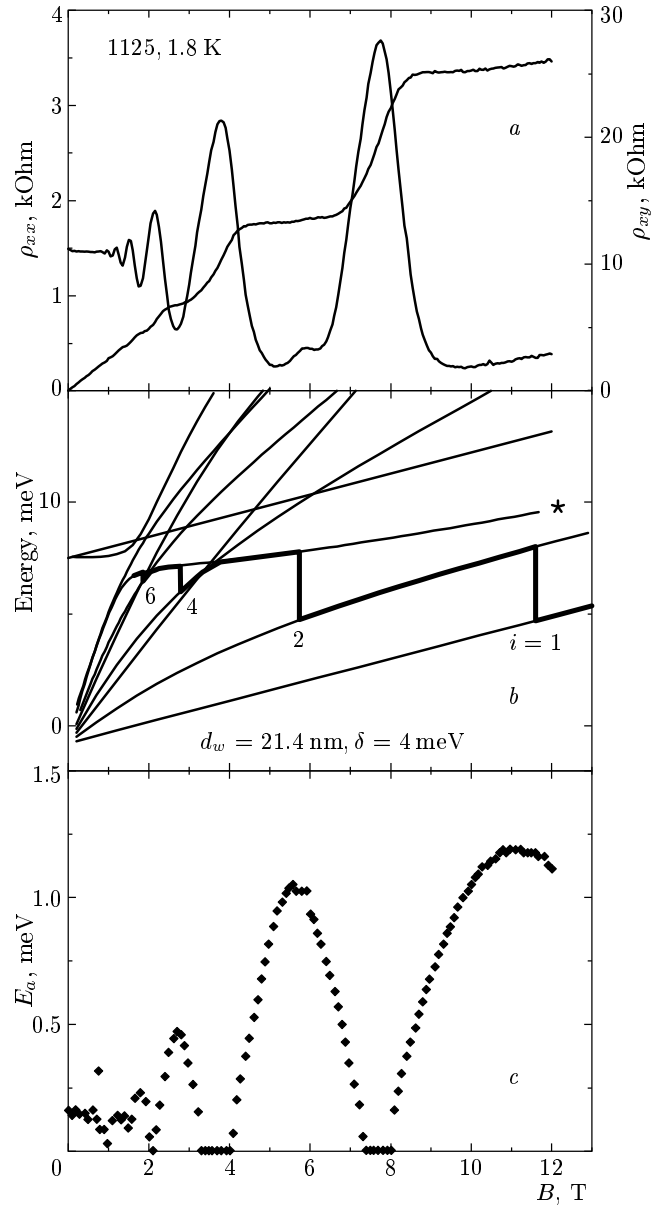


Fig. 1. Comparison of the calculated LL picture and the Fermi level motion (b) with the experimental recordings (a) and deduced activation energies (c) for sample 1125a₇. Mobility gaps are estimated from (c) as twice the maximum $E_a(B)$ values

1–1.7 $\text{m}^2/\text{V}\cdot\text{s}$. The double cross Hall bridges were fabricated by the photolithography and subsequent wet etching technique and contacts attached by the thermocompression. Hall and longitudinal magnetoresistivities were measured on the dc current in normal magnetic fields up to 12 T in the steady regime and up to 32 T in ~ 10 ms pulses within the temperature range $0.1 \text{ K} \leq T \leq 15 \text{ K}$.

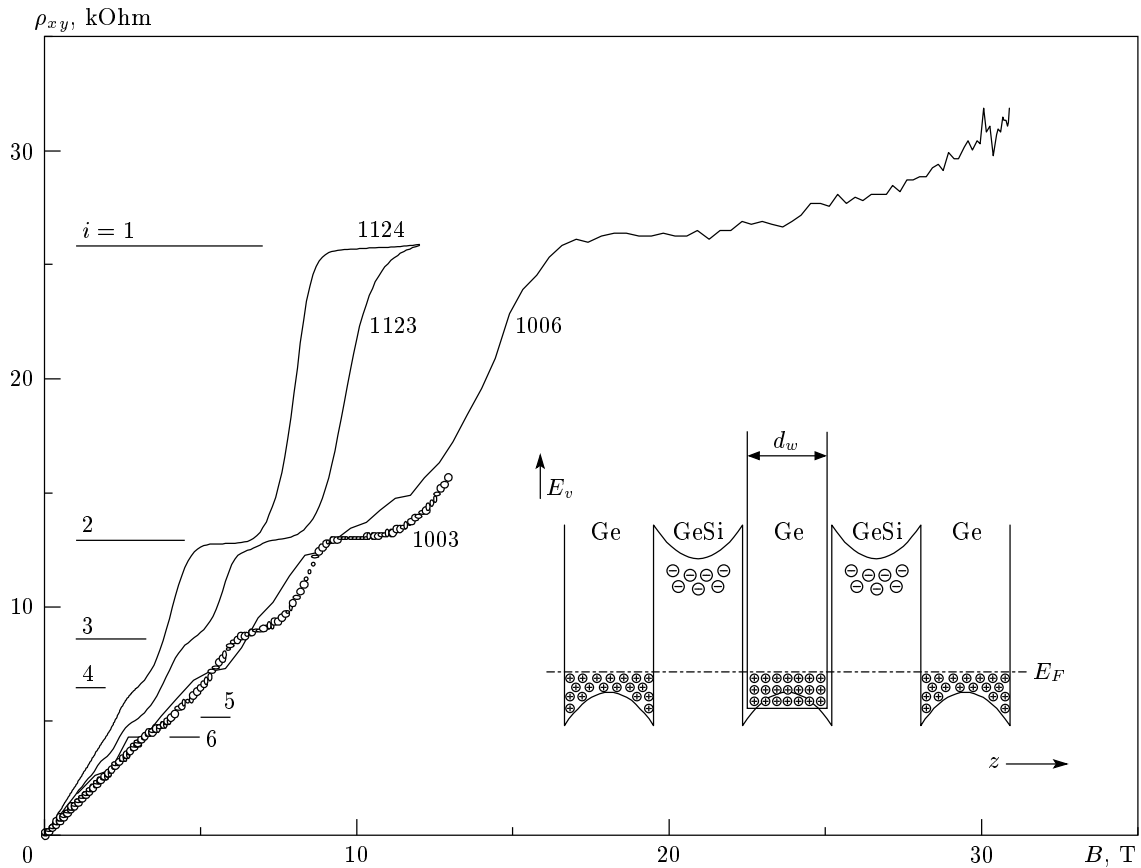


Fig. 2. Quantum Hall effect in different samples. Inset: a schematic valence band energy diagram of the samples studied

3. GENERAL PICTURE OF LANDAU LEVELS DEDUCED FROM THE QUANTUM HALL EFFECT

3.1. Manifestations of the second subband in $\rho_{xx}(B)$ and $\rho_{xy}(B)$ experimental traces

The simplest situation occurs for the narrowest Ge layers with the lowest hole densities. In this case, the QW profile approaches a rectangular shape and only the lowest confinement subband is filled with holes. Although the system of Landau levels in the valence band is rather complicated [4] due to heavy and light hole hybridization complemented by the effects of confinement and uniaxial stress (Fig. 1b), the experimental recordings of the longitudinal and Hall magnetoresistivities, $\rho_{xx}(B)$ and $\rho_{xy}(B)$, have a regular structure similar to that observed in a simple nondegenerate conduction band (Fig. 1a). The $\rho_{xy}(B)$ traces contain plateaux of the integer quantum Hall effect (QHE) at fundamental values $\rho_{xy} = h/ie^2$, with i an integer, concomitant with minima in $\rho_{xx}(B)$, both kinds of peculiarities being regularly spaced in the reciprocal magnetic field

Sample parameters

Sample	μ , $\text{m}^2/\text{V}\cdot\text{s}$	p_s , 10^{15} m^{-2}	d_w ,* nm	$p_s d_w^2$
1006-1	1.4	4.9	12.5	0.77
1124 b ₃	1.0	2.8	20 (21.4)	1.28
1125 a ₇	1.7	2.8	20 (22)	1.36
1123 a ₆	1.4	3.4	20 (23.5)	1.88
1003-2	1.5	4.8	22	2.32

* In brackets, we present the corrected values obtained from our analysis.

and monotonously damped with decreasing the field. The peculiarities correspond to $i = 1, 2, 4, 6, \dots$, i.e., the even numbered QH peculiarities dominate at weak fields. This is analogous to a simple conductivity band for small Zeeman splitting.

Magnetoresistivities of an entirely different structure were detected for samples with wider Ge layers

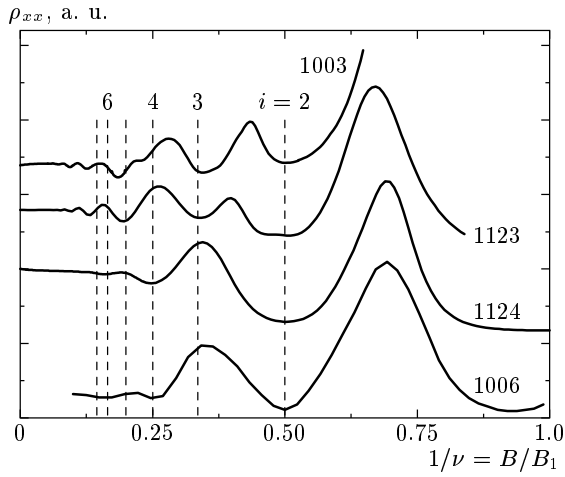


Fig. 3. Longitudinal magnetoresistivity of the samples shown in Fig. 2, scaled versus the inverse filling factor

and higher hole densities [5]. In Figs. 2 and 3, the Hall and longitudinal magnetoresistivities are depicted for the samples presented in the Table. For the longitudinal magnetoresistivity, the amplitudes of the traces are normalized to the highest peak and in their positions are normalized by scaling them versus the inverse filling factor $\nu = p_s h/eB$. The common feature of these five samples is that in spite of different QW widths and hole densities, their traces contain plateaux in $\rho_{xy}(B)$ and concomitant $\rho_{xx}(B)$ minima for $i = 1$ and 2. But the structures of these curves differ significantly below the plateau with $i = 2$.

For samples 1006, 1124, and 1125, the plateau with $i = 4$ comes next on the low-field side after the plateau with $i = 2$ and the other even numbered plateaux dominate. For the other two samples, 1123 and 1003, the plateau with $i = 3$ comes next after the one with $i = 2$, the plateau with $i = 4$ is missed, and the odd numbered plateaux dominate. These features are even more pronounced in the $\rho_{xx}(B)$ curves (Fig. 3). To explain this, we have calculated the Ge valence band energy spectra quantized by both the magnetic field and the confinement. The model of an infinitely deep rectangular well was used [4]. Examples of these calculations are presented in Figs. 1b and 4. The behavior of the Fermi level is presented for extremely sharp LLs and constant total hole densities.

The calculations show that in sample 1006, the Fermi level moves within the ground confinement subband. Its levels are grouped in pairs, similarly to the LL picture for the conduction band with a small spin splitting. This is why the even-numbered peculiarities dominate here.

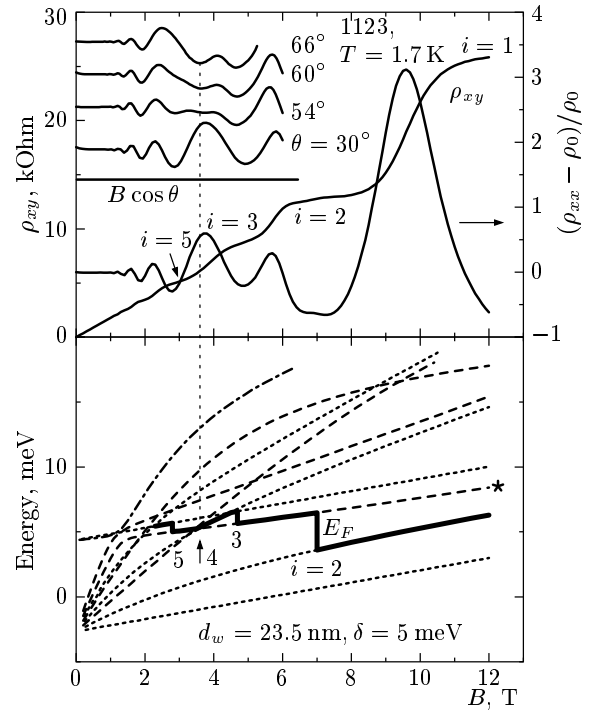


Fig. 4. Radical changes in the structure of QHE due to involvement of the second subband

With lowering the magnetic field, the Fermi level approaches the lowest LL of the second subband (the level marked with «*» in Figs. 1b and 4). In samples 1124 and 1125, it enters this LL, but this event does not lead to essential changes in the experimental recordings (Figs. 1a, b).

The degree of the second subband involvement increases with $p_s d_w^2$, and the samples in the Table are sorted in rows according to this parameter. As follows from the calculations (Fig. 4), the value of $p_s d_w^2 \approx 1.9$ for sample 1123 is sufficient for the Fermi level to rather deeply penetrate the second subband; as a result, a single step for $i = 2$ in the Fermi level motion between the ground subband LLs is divided into two steps with $i = 2$ and $i = 3$. This is how the $i = 3$ peculiarity arises in the experimental data.

Another consequence of the embedding the additional level is that step number 4 for sample 1123 no longer corresponds to the transition at the distance of about the cyclotron energy between the orbitally split spin couples of the ground subband; instead, it corresponds either to the transition onto this additional level or, if the embedded level is lower than the Fermi level, to the transition within the spin split couples. In the latter case, the numbers of the observed peculiarities, i.e., the corresponding integer filling factors, are merely

shifted one unit higher because of an additional level emerging below the Fermi level (changing their numbers from even to odd ones). In both cases, the energy distance for the $i = 4$ peculiarity can become much smaller than the cyclotron energy, leading to its disappearance. The crucial role of the second confinement subband position relative to the Fermi level is therefore evident. On the other hand, this position is very sensitive to the width and the shape of the QW, which should be reflected in a high sensitivity of the structure of experimental curves to diverse changes in the system. Indeed, in sample 1003 with parameters not strongly different from those of sample 1123, a small peculiarity with $i = 4$ has been detected. In the inset in Fig. 4, we show the evolution of magnetoresistivity of sample 1123 with a tilt of the magnetic field from the normal to the sample plane. The tilt introduces some changes into the LL picture that revive the peculiarity with $i = 4$, initially absent.

3.2. Activation magnetotransport in the quantum Hall mobility gaps

It is now commonly accepted that the existence of quantized plateaux in the $\rho_{xy}(B)$ dependences with vanishing values of ρ_{xx} is caused by the existence of disorder-induced mobility gaps in the DOS of a 2D system. When the Fermi level is settled down in the gap, the thermally activated behavior of ρ_{xx} (or σ_{xx}) is observed due to the excitation of electrons to the narrow band of extended states (with a width γ) near the middle of a disorder-broadened LL.

As a rule, it is assumed that the delocalized states have discrete energies $E = E_N$ separated by the (mobility) gap $\Delta \gg k_B T$, which leads to the expression [6–9]

$$\sigma_{xx} \propto \exp\left(-\frac{E_a}{k_B T}\right), \quad (1)$$

where $E_a = |E_F - E_N|$. In the valence band of 2D Ge, a nonlinear dependence of LLs on the magnetic field results in that the strong inequality $\Delta \gg k_B T$ is not valid even at fields as high as $B \approx 10$ T and a more general expression must be used for the temperature-dependent conductivity $\sigma_{xx}(T)$:

$$\sigma_{xx}(T) = \int \sigma(E) \frac{\partial f(E)}{\partial E} dE. \quad (2)$$

Here, $f(E)$ is the Fermi–Dirac distribution function and $\sigma(E)$ is a partial conductivity at the energy E . For an extremely narrow band of delocalized states ($\gamma \ll k_B T$), Eq. (2) yields

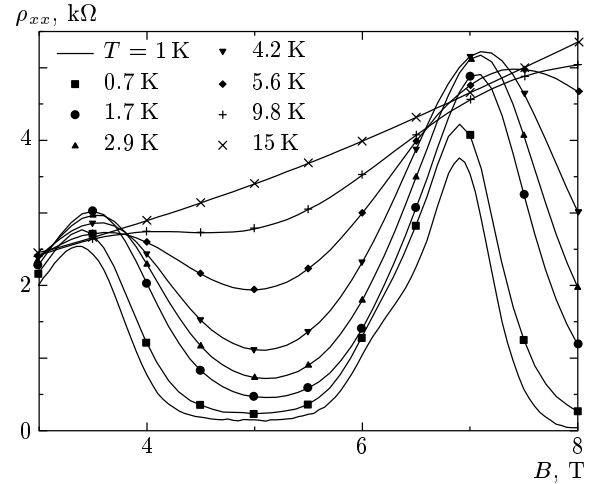


Fig. 5. Variations of the magnetoresistivity with the temperature

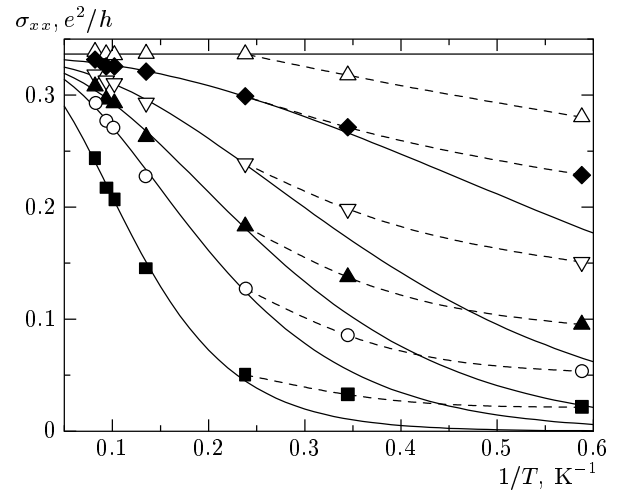


Fig. 6. Activation behavior of the conductivity: $B = 8$ (Δ), 8.2 (\blacklozenge), 8.5 (∇), 8.8 (\blacktriangle), 9.2 (\circ), 11.2 T (\blacksquare)

$$\sigma_{xx}(T) = \sigma_0 \frac{\gamma}{k_B T} \left. \frac{\partial f(E)}{\partial E} \right|_{E=E_a}, \quad (3)$$

where σ_0 is of the order of the minimal metallic conductivity.

In the structures investigated, the magnetoresistivity was measured (Fig. 5) and the thermally activated conductivity was found in the range $T = (3–15)$ K for fixed values of B in the quantum Hall plateau regions, see Fig. 6. The solid curves correspond to expression (3) with E_a and γ as fitting parameters ($\sigma_0 = 0.5e^2/h$). Deviations of the experimental points from the calculated curves for $T < 3$ K (connected by lines as guides to the eye in Fig. 6) are explained by variable range

hopping among localized states at E_F , which usually dominates for sufficiently low T .

The activation energy E_a is presented in Figs. 1c and 7 as a function of B or the filling factor ν in the vicinity of $\nu = 1, 2$, and 4 for two of the investigated samples. The activation energy achieves its maximum value E_a^{max} at integer values of ν . The mobility gap width estimated as $\Delta = 2E_a^{max}$ is close to the energy separation $\Delta \approx |E_N - E_{N'}|$ between the adjacent LLs within the uncertainty of the order of γ . In a simple parabolic band, the activation energy for the integer filling factor corresponds to half the cyclotron energy, $E_a^{max} \approx \hbar\omega_c/2$ [8, 9]. Because of a pronounced sub-linearity in the B dependence of the valence band energy levels (Figs. 1b and 4) and the interference with the second subband levels, estimations of the cyclotron energy from the low-field Shubnikov–de Haas oscillations may strongly contradict the inter-LL distances obtained from the activation analysis in high fields. Thus, $\hbar\omega_c$ should be about 10 meV at $B = 10$ T for samples 1124 and 1125 with the value $m = 0.1m_0$ obtained from oscillations, while we have found $\Delta = (2.4\text{--}2.6)$ meV and $\Delta = (1.8\text{--}2.2)$ meV for $\nu = 1$ and 2, respectively, from the activation conductivity.

Considering that the mobility gap corresponds to most of the inter-LL distance, leaving just an infinitesimal part for the stripe of delocalized states in the middle of LLs, the values of mobility gaps thus obtained can be compared with the calculated inter-LL distances. In comparison with a qualitative analysis of the structure of experimental magnetoresistivity traces described in the preceding paragraph, the activation analysis yields a quantitative tool to probe inter-LL distances.

An example of such an analysis for sample 1125a₇ is presented in Fig. 1, where the steps in the Fermi level motion with the magnetic field due to jumps between the calculated LLs are juxtaposed with both the experimental recordings and the deduced activation energies. While a pronounced step in $E_F(B)$ indicates only the existence of QH peculiarities in $\rho_{xx}(B)$ and $\rho_{xy}(B)$, a quantitative analysis can be done on the basis of the deduced activation energies. Thus, we can note that if the entire process were developed in the first subband, then the $i = 2$ mobility gap would be about 30% wider than that for $i = 1$ (Fig. 1b). The ratio of the gap for $i = 2$ to that for $i = 1$ is reduced by fitting the obtained activation energies when the second confinement subband is considered. We achieved the best coincidence for sample 1125 by taking the Ge layer width $d_w = 21.4$ nm, slightly higher than the nominal value 20.0 nm.

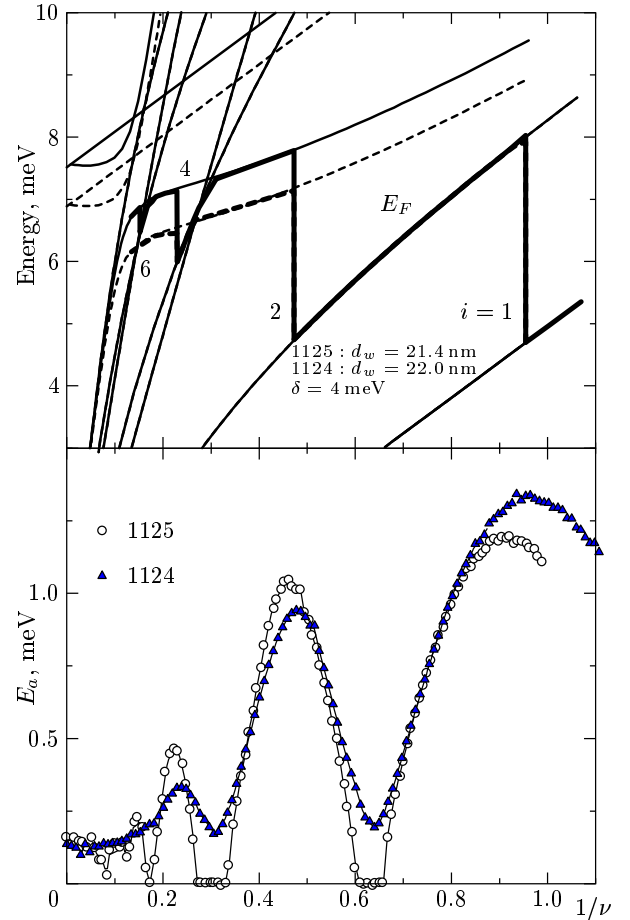


Fig. 7. Activation energies for sample 1125 compared with the data for sample 1124 (bottom) and explanation of the difference by the involvement of the second confinement subband (top: solid lines for 1125 and dashed ones for 1124)

Involvement of the second subband offers a possibility to explain the difference between the activation energies in samples 1125 and 1124 with nominally similar parameters. For the latter sample, the ratio of the mobility gap for $i = 2$ to the one for 1 is about a quarter lower than for the former (Fig. 7, lower part). As seen from the quantized structure of the 2D Ge valence band in the upper part of Fig. 7, the decrease of the mobility gap ratio in sample 1124 may be explained by some lowering of the second subband (dashed lines for LLs and Fermi energy in Fig. 7) due to an increase of the Ge layer width. The necessary correction to the Ge layer width is small, from 21.4 to 22.0 nm, due to a strong (approximately quadratic) sensitivity of the second subband energy to the layer width.

4. SCANNING THE DENSITY OF STATES BETWEEN AND WITHIN THE LANDAU LEVELS

The nature of the QHE is known to be closely related to the electron localization phenomenon in 2D disorder systems at quantizing magnetic fields. For the QHE to exist, narrow bands of extended states must be present close to the center of each of the Landau subbands provided that all the other states are localized [10, 11]. When the magnetic field values are in the plateau regions, the system is in the localized regime and the temperature dependence of the dissipative conductivity σ_{xx} (and the resistivity $\rho_{xx} \approx \sigma_{xx}/\sigma_{xy}^2$) is of an exponential character, $\sigma_{xx}(T) \rightarrow 0$ as $T \rightarrow 0$ [7, 8]. If the magnetic field is in the plateau–plateau (PP) transition region, the Fermi level passes through the narrow strip of extended states at the Landau level center and the system behaves as a metal with nonzero conductivity as $T \rightarrow 0$ and a peak-like form of the $\sigma_{xx}(B)$ dependence.

This section is organized as follows. The results for the QHE plateau regions are presented in Sec. 4.1, where the background density of localized states is evaluated from the analysis of activated magnetoresistivity. Two random impurity potential models are used for evaluation of the impurity potential fluctuation parameters, the random potential amplitude and the nonlinear screening length in the vicinity of integer filling factors (FFs). In Sec. 4.2, the data for the QHE PP transition regions are reported and the temperature dependence of the width of the extended state band is extracted and analyzed in terms of the theory of critical phenomena. The effect of the Coulomb interaction on smooth disorder potential screening is discussed.

4.1. The density of states in the mobility gap

The DOS in mobility gaps can be evaluated from the data on the activation energy E_a as a function of the LL filling factor $\nu = n/n_B$ (where n is the electron density and $n_B = eB/hc$). The filling factor can be tuned by the change of either the carrier density [6] or the magnetic field [7–9]. We use the method of activated magnetoresistivity for the reconstruction of the 2D-hole gas DOS under quantizing magnetic fields in the p -Ge/Ge_{1-x}Si_x system. The DOS was calculated taking thermal activation of both electrons and holes on adjacent LLs into account [6, 12].

From the $E_a(B)$ dependences, the density of lo-

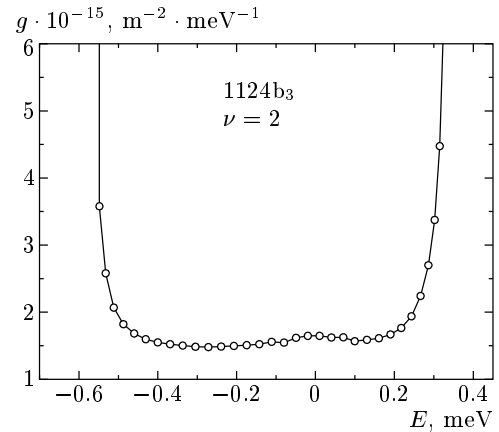


Fig. 8. The background density of states for sample 1124, as deduced from the activation energy; $E = 0$ corresponds to the middle of the energy interval between two LLs

calized states in the mobility gap can be constructed as [8, 9]

$$g(E_F) = \left[\frac{dE_a(n)}{dn} \right]^{-1} = \frac{\nu e}{2\pi\hbar c} \left(\frac{dE_a(B)}{dB} \right)^{-1}. \quad (4)$$

In Fig. 8, we show the typical results for the mobility gap DOS as a function of energy. Even in the middle of the gap, the density of localized states was found to have an unexpectedly high value, comparable to that for two filled confinement subbands without the magnetic field, $g_0 = m/(\pi\hbar^2) \approx 1 \cdot 10^{15} \text{ m}^{-2} \cdot \text{meV}^{-1}$. Moreover, $g(E)$ is practically independent of E in the overwhelming part of the energy interval between adjacent LLs: $g(E) = g_c = (1-1.5) \cdot 10^{15} \text{ m}^{-2} \cdot \text{meV}^{-1}$ for $\nu = 1$ and 2. This result is consistent with those obtained for AlGaAs/GaAs [8, 9], InGaAs/InP [7] heterostructures and Si-MOSFET structures [6] with the n -type conductivity.

Because all the short-range impurity potential models lead to an exponential drop in the DOS between Landau levels, a clear picture of the DOS in the QHE regime can be presented only in terms of the long-range potential fluctuations in combination with the oscillating dependence of the DOS on the filling factor. This idea was advanced in the early work by Shklovskii and Efros [13] and was later developed in a series of works by Efros et al. (see [14, 15] and references therein). In a selectively doped heterostructure, the smooth random potential is formed by fluctuations in the concentration of remote impurities.

For a random potential $V(r)$, which is smooth at the scale of the magnetic length l_B , the localization in the

QHE regime can be discussed in terms of semiclassical quantization and percolation [16]. In the semiclassical limit, the electron energy in the quantizing magnetic field can be written as

$$E_N(r_0) = \hbar\omega_c \left(N + \frac{1}{2} \right) + V(r_0), \quad (5)$$

where r_0 is the oscillator center coordinate. A smooth potential therefore removes the degeneracy in r_0 and makes the LL energy dependent on spatial coordinates.

An order of magnitude evaluation of the spatial scale and amplitude of the random potential in $p\text{-Ge}/\text{Ge}_{1-x}\text{Si}_x$ heterostructures in the QHE regime can be obtained from the analysis of the mobility gap DOS. Two models for the random impurity potential were used.

i) The model with randomly distributed charged centers located within a thick layer close to the $2D$ electron (hole) gas [13], for which the relation between the fluctuation amplitude F and scale L is

$$F(L) = \beta \frac{e^2 \sqrt{NL}}{\kappa}, \quad (6)$$

where β is a numerical coefficient ($\beta \approx 0.1$ [14]), N is the density of charged impurities (per volume), and κ is the static dielectric constant.

ii) The model of the system with a spacer: a condenser with the $2D$ electron (hole) gas as one plate and randomly distributed charged centers as the other plate, separated by a distance d_s [14, 15]. In this case,

$$F(L) = \frac{e^2 \sqrt{2\pi C}}{\kappa} \sqrt{\ln \frac{L}{2d_s}}, \quad (7)$$

where C is the average impurity density (per area).

It can be seen from Eqs. (6) and (7) that without screening, the amplitude F diverges at large L . When the filling factor is close to an integer (i), a very small concentration of electrons $\delta n \ll n_B$ can be redistributed in space, and the so-called nonlinear screening [13–15] occurs (the «threshold» screening [17]). For $\nu = i$ exactly, the screening is realized only due to electrons and holes induced by an overlap of the adjacent fluctuating Landau levels, and the random potential amplitude is therefore of the order of the corresponding LL gap.

For the investigated heterostructures, $N \approx 10^{23} \text{ m}^{-3}$ ($C = Nd_a \approx 10^{15} \text{ m}^{-2}$) and the mean distance between impurities $N^{-1/3} \approx 20 \text{ nm}$ is comparable to both the width of $2D$ Ge layer $d_w \approx 20 \text{ nm}$ and the width of the doped part of the sample $d_a \approx 10 \text{ nm}$. Thus, the described models are not valid precisely,

but are suitable to obtain a range of random potential parameter values.

In the nonlinear screening regime, the respective DOS in the middle of the mobility gap [13–15] of width $W \approx 2 \text{ meV}$ for the two models are given by

$$\text{i) } g\left(\frac{W}{2}\right) = \frac{4\beta e^2 N}{\kappa W^2} \approx 7.5 \cdot 10^{10} \text{ cm}^{-2} \cdot \text{meV}^{-1}, \quad (8)$$

$$\text{ii) } g\left(\frac{W}{2}\right) = \frac{2\sqrt{C}}{7Wd_s} \approx 9.5 \cdot 10^{10} \text{ cm}^{-2} \cdot \text{meV}^{-1}. \quad (9)$$

Without any fitting parameter, we therefore obtain a rather reasonable evaluation of the background DOS, and the two models yield values close to each other. For the random potential amplitude comparable to the mobility gap, $F \approx W$, we obtain the nonlinear screening length (the scale of optimum fluctuation) $L_c \approx 100 \text{ nm}$ for model (i) (see Eq. (6)) and $L_c \approx 40 \text{ nm}$ for model (ii) (see Eq. (7)). We see that in both cases, the spatial scale of fluctuations is essentially larger than the magnetic length ($l_B \approx 8 \text{ nm}$ at $B = 10 \text{ T}$), and therefore, the random potential can indeed be regarded as a smooth one.

Therefore, order-of-magnitude evaluations of the random impurity potential parameters for the $p\text{-Ge}/\text{Ge}_{1-x}\text{Si}_x$ heterostructures indicate that in the vicinity of integer filling factors $\nu = 1$ and $\nu = 2$ (i.e., in the regions of QHE plateaux), a sharp broadening of LL occurs. It is believed that for the filling factor close to a half-integer (the regions of the plateau-plateau transition), the potential fluctuations must be small because of the effective (linear) electron screening [13–15].

4.2. The width of the extended state band

The QHE regime can be regarded as a sequence of quantum phase insulator–metal–insulator transitions when the DOS of the $2D$ system in quantizing magnetic fields is scanned by the Fermi energy. In accordance with this concept, the transition regions between the adjacent QHE plateaux, as well as the widths of the appropriate $\rho_{xx}(B)$ peaks, must become narrower as the temperature approaches zero. In the theoretical framework of scaling (see, e.g., [18] and references therein), the width of the transition regions tends to zero as

$$\delta B_{i \rightarrow (i+1)} \propto T^\kappa, \quad (10)$$

where $\kappa = 1/z\nu$, $\nu = 7/3$ is the critical index of localization length, and $z = 1$ is the dynamical critical index.

The pioneer experimental study on low-mobility InGaAs/InP heterostructures by Wei et al. [19] has strongly supported the power-law behavior in Eq. (10). The evolution of the width of the ρ_{xx} peaks and of the inverse maximal slope of the ρ_{xy} steps, $(d\rho_{xy}/dB)_{max}^{-1}$, as a function of the temperature, corresponds to (10) with a nearly universal value of the exponent $\kappa = 0.4 \pm 0.04$ for several LLs. The scaling behavior with $\kappa = (0.42\text{--}0.46)$ was later reported for the QHE plateau–plateau transition in GaAs/AlGaAs heterostructures [20] and in *p*-SiGe quantum wells [21] and for the QHE-to-insulator transition in GaAs/AlGaAs [20] and InGaAs/InP heterostructures [22].

In other series of experimental works, the universality of the exponent κ was questioned (see references in review article [16]). For instance, the measured values of κ increased from 0.28 to 0.81 with decreasing mobility in AlGaAs/GaAs heterostructures [23] or the values of κ between 0.2 and 0.65 were obtained for six subbands of Si-MOSFETs [24].

In a recent work by Shahar et al. [25], a novel transport regime distinct from the critical scaling behavior was reported to exist asymptotically close to the transition at very low temperatures. Studying the QHE-to-insulator transition in a variety of GaAs/AlGaAs and InGaAs/InP samples at temperatures down to 70 mK, they found an exponential dependence of ρ_{xx} on the filling factor on both sides of the critical FF value ν_c ($\Delta\nu = |\nu - \nu_c|$),

$$\rho_{xx} = \exp(-\Delta\nu/\nu_0(T)), \quad (11)$$

and emphasized that the effective transition width $\nu_0(T)$ appears to vary as $\alpha T + \beta$ rather than to exhibit the T^κ scaling behavior. This implies that even at $T = 0$, the transition is of a finite width unless a different conduction mechanism takes over at even lower temperatures. The authors noted that some of their InGaAs/InP samples were from the same growth as the sample in Ref. [19] and that they also revised their own previous data for GaAs/AlGaAs samples [20].

To estimate the width of the band of delocalized states in our Ge/Ge_{1-x}Si_x samples, we have analyzed the magnetoresistance data in the transition region between the first and the second QHE plateaux in two ways. First, we used the description of $\sigma_{xy}(B)$ dependences in terms of the so-called scattering parameter [26]

$$s = \exp(-\Delta\nu/\nu_0(T)). \quad (12)$$

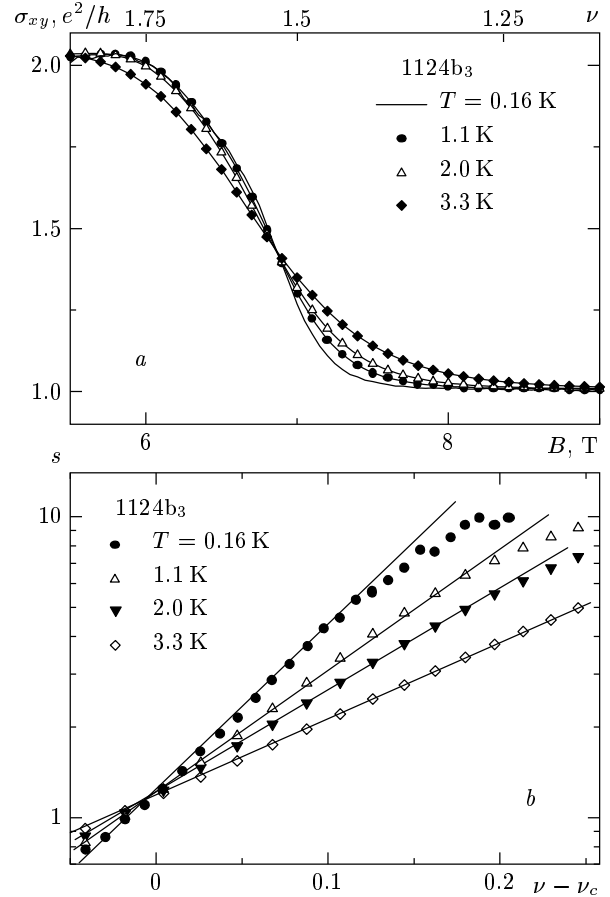


Fig. 9. Hall conductivity for sample 1124b₃ (a), plotted as a function of filling factor ν and scattering parameter s (b). The latter is derived from the σ_{xy} data shown in (a)

For the $1 \rightarrow 2$ plateau–plateau transition, the scattering parameter can be extracted as [21, 27]

$$\sigma_{xy} = 2 - s^2/(1 + s^2). \quad (13)$$

The other way that we used was to find the maximum slope of $(d\rho_{xy}/dB)_{max}$ in a transition region and to draw its inverse in reliable units against the temperature as in Ref. [19].

In Figs. 9a, b, we show the $\sigma_{xy}(B)$ and $s(\nu)$ dependences for one of the investigated samples, 1124b₃. Figures 10a, b depict the $\nu_0(T)$ dependences extracted in accordance with Eq. (12) in a log-log graph and on a linear scale. It can be seen from Fig. 10a that the data cannot be satisfactorily described by a power law $\nu_0 \rightarrow T^\kappa$ (it is not the straight line on the log-log plot). On the other hand, the data are much more compatible with the linear dependence

$$\nu_0(T) = \alpha T + \beta \quad (14)$$

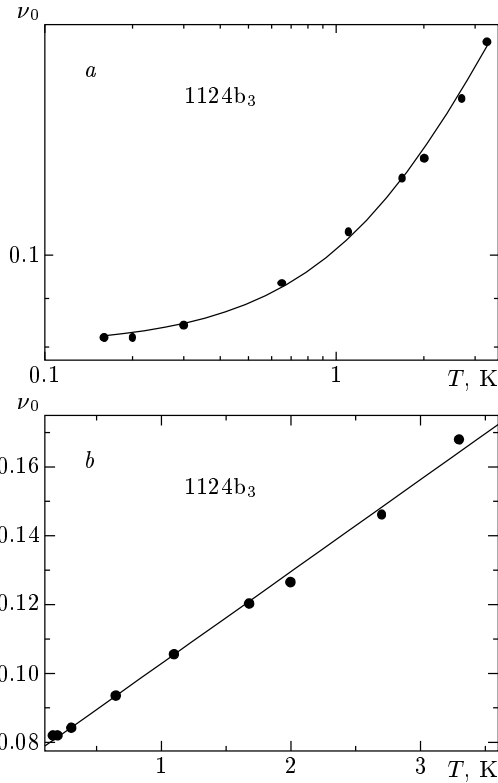


Fig. 10. *a*) A log–log graph of $\nu_0(T)$ in Eq. (12), plotted against T . *b*) The same as (*a*), plotted using a linear graph. Solid lines are the best fit

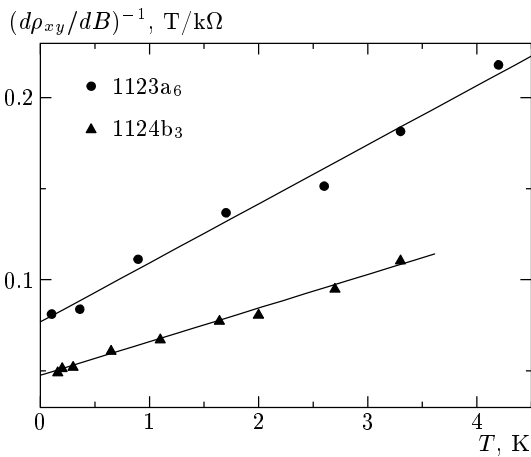


Fig. 11. The inverse maximum slope of $(d\rho_{xy}/dB)^{-1}_{max}$ as a function of temperature for two samples 1123a₆ and 1124b₃

with $\alpha = 0.076$, $\beta = 0.027$, and $\beta/\alpha = 2.8$ K (Fig. 10b).

Qualitatively, the frontal treatment of the data by the inverse maximum slope of $\rho_{xy}(B)$ yields the same but slightly less accurate result in Eq. (14) with

$\beta/\alpha = 2.6$ K for sample 1124b₃ and $\beta/\alpha = 2.3$ K for sample 1123a₆ (Fig. 11).

As pointed out in [25], the ratio β/α defines a temperature T^* that is found to be characteristic of the material system. Thus, T^* occurred to be close to 0.5 K for InGaAs/InP samples and 50 mK for GaAs/AlGaAs samples [25]. It can be seen that the characteristic temperature is about 2.5 K (2.3–2.8 K) for Ge/GeSi samples studied here.

In the theoretical work by Pruisken et al. [28] and in the experimental work by van Schaijk et al. [22], it is emphasized that short-range random potential scattering is essentially important in studying scaling phenomena because the long-range potential fluctuations dramatically complicate their observability. In their opinion, the linear behavior ($\nu_0 = \alpha T + \beta$) is semiclassical in nature and should be observed at finite T and in samples with predominantly slowly varying potential fluctuations.

The simplest and most natural reason for the linear $\nu_0(T)$ dependence, namely, the thermal broadening of a quantum critical phase transition, is suggested and confirmed by calculations in the work by Coleridge and Zawadzki [27]. It is shown there that the thermal broadening not only yields the linear increase in $\nu_0(T)$ but also leads to a temperature-dependent increase of the σ_{xx} peak height as the temperature is lowered. This was observed in their experiment.

There is nothing about the temperature dependence of ρ_{xx} (or σ_{xx}) peak value in the work by Shahar et al. [25]. But we observe a linear $\nu_0(T)$ dependence in Ge/GeSi samples within the temperature interval where the peak values of σ_{xx} undoubtedly decrease with lowering T (Fig. 12). Then we are not in the conditions of thermal broadening, in contrast to the experiment in [27].

We believe that the answer to the main question about the finite width of QHE transitions as $T \rightarrow 0$ can be found in the works treating the effect of Coulomb interactions on the screening of smooth disorder potentials [29–31]. The theory involves screening within the Thomas–Fermi approximation appropriate for a smooth disorder.

The effect of the electron–electron interaction manifests in that the regions of the third kind occur in the sample in addition to the local areas of filled and empty LLs present in the noninteracting system. The new «metallic» regions are those where the local electron density is between zero and that of the filled LL. The percolation description must then be revised because the metallic region percolates through the sample over a finite range of magnetic field near the critical

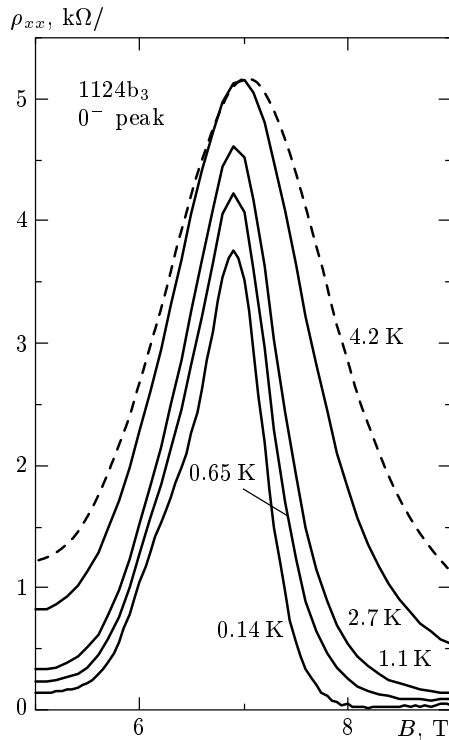


Fig. 12. The $0^- \rho_{xx}^{peak}$ value for sample 1124b₃ at different temperatures

value. We therefore expect the transition between Hall plateaux to have a finite width in filling factors even in the low-temperature limit.

It is notable that the value of $\nu_0(T \rightarrow 0)$ gives an empirical estimate of the fraction of extended states in the total number of states per magnetic quantum level $n_B = eB/hc$.

We have $\nu_0(T \rightarrow 0) = 0.08$ for the 0^- LL in sample 1124b₃ (see Fig. 10b). It can be seen that a tiny part of states is extended, i.e., most of them are localized, as it should be in the QHE regime.

5. CONCLUDING REMARKS

Scanning the quantized valence band of the Ge layers by the Fermi level in the quantum Hall regime yields opportunities to reconstruct the Landau level pattern of the band, including the levels at the bottom of the second confinement subband, to feel the shift of the second subband introduced by tiny changes in the QW profile. Furthermore, this experimental approach allows going beyond the model of delta-shaped LLs and investigating the distribution of localized and extended states throughout the entire LL picture in detail.

In selectively doped p -Ge/Ge_{1-x}Si_x heterostructures investigated here, the main scattering mechanism for quasi-2D holes in Ge quantum wells at low temperatures is the scattering on remote ionized boron impurities located at Ge_{1-x}Si_x barriers. The fluctuations in the density of randomly distributed remote impurities act as a source of the smooth disorder potential causing localization effects in the quantum Hall regime. Screening of this disorder assumes a very different character depending on the value of the filling factor. When the Fermi level is near the center of the Landau subband (half-integer filling factors), electrons are free to adjust their density and screening of random potential is good, but when it lies in the mobility gap between LLs (nearly integer filling factors), they cannot, and screening is poor.

We could explain the unusually high values of the background DOS obtained from the analysis of thermally activated magnetoresistance in the QHE plateau regions in the vicinity of $\nu = 1$ and $\nu = 2$ only in the framework of disorder potential, smooth at the scale of the magnetic length. In the models with nonlinear screening of a long-range random impurity potential, we obtain a reasonable estimate both for the density of localized states and for the spatial scale of potential fluctuation, which actually occurs to be rather large compared with the magnetic length.

On the other hand, for half-integer filling factors, the linear temperature dependence of the effective QHE plateau-plateau transition width $\nu_0(T) = \beta + \alpha T$ is observed in our Ge/Ge_{1-x}Si_x samples in contrast to the scaling behavior inherent to systems with a short-range disorder. This result is in accordance with the data of recent experimental work [25] for other semiconductor systems. It is tempting to consider the finite width of the QHE transition, even as $T \rightarrow 0$, as a consequence of an effective screening of smooth random potential due to the Coulomb repulsion of electrons [29–31].

The work is supported by the Russian Foundation for Basic Research, projects 02-02-16401, 01-02-17685, 02-02-06864, and 02-02-06168; INTAS YSF 01/1-156, and the 6-th concurs-expertise RAS (1999) № 68.

REFERENCES

1. F. Schaffler, *Semicond. Sci. Technol.* **12**, 1515 (1997).
2. C. M. Engelhard, D. Toebben, M. Aschauer et al., *Sol. St. Electron.* **37**, 949 (1994).

3. R. Winkler, M. Merkler, T. Darnhofer, and U. Rössler, *Phys. Rev. B* **53**, 10858 (1996).
4. Yu. G. Arapov, N. A. Gorodilov, V. N. Neverov, M. V. Yakunin et al., *Pis'ma Zh. Eksp. Teor. Fiz.* **59**, 247 (1994).
5. Yu. G. Arapov, V. N. Neverov, G. I. Harus, N. G. Shelushinina, M. V. Yakunin, and O. A. Kuznetsov, *Semiconductors* **32**, 649 (1998).
6. M. G. Gavrilov and T. V. Kukushkin, *Pis'ma Zh. Eksp. Teor. Fiz.* **43**, 79 (1986).
7. H. P. Wei, A. M. Chang, D. C. Tsui, and M. Rozeghi, *Phys. Rev. B* **32**, 7016 (1985).
8. D. Weiss, E. Stahl, G. Weiman et al., *Surf. Sci.* **170**, 285 (1986).
9. P. Svoboda, G. Nachtwei, C. Breitlow et al., E-print archives, cond-mat/9612053.
10. R. B. Laughlin, *Phys. Rev. B* **23**, 5632 (1981).
11. B. I. Halperin, *Phys. Rev. B* **25**, 2185 (1982).
12. Yu. G. Arapov, G. I. Harus, V. N. Neverov, N. G. Shelushinina, M. V. Yakunin, G. A. Alshanskii, and O. A. Kuznetsov, *Nanotechnology* **11**, 351 (2000); E-print archives, cond-mat/0103343.
13. B. I. Shklovskii and A. L. Efros, *Pis'ma Zh. Eksp. Teor. Fiz.* **44**, 520 (1986).
14. A. L. Efros, *Sol. St. Comm.* **70**, 253 (1989).
15. A. L. Efros, F. G. Pikus, and V. G. Burnett, *Phys. Rev. B* **47**, 2233 (1993).
16. B. Huckestein, *Rev. Mod. Phys.* **67**, 357 (1995).
17. I. V. Kukushkin, S. V. Meshkov, and V. B. Timofeev, *Uspekhi Fiz. Nauk* **155**, 219 (1988).
18. D. Liu and S. Das Sarma, *Phys. Rev. B* **49**, 2677 (1994).
19. H. P. Wei, D. C. Tsui, M. A. Paalanen, and A. M. M. Pruisken, *Phys. Rev. Lett.* **61**, 1294 (1988).
20. D. Shahar, D. C. Tsui, M. Shayegan, E. Shimshoni, and S. L. Sondhi, E-print archives, cond-mat/9611011.
21. P. T. Coleridge, E-print archives, cond-mat/9902103.
22. R. T. F. van Schaijk, A. de Visser, S. Olsthoorn, H. P. Wei, and A. M. M. Pruisken, *Phys. Rev. Lett.* **84**, 1567 (2000); E-print archives, cond-mat/9812035.
23. S. Koch, R. J. Haug, K. von Klitzing, and K. Ploog, *Phys. Rev. B* **43**, 6828 (1991).
24. M. D'Iorio, V. M. Pudalov, and S. M. Semenchinsky, in *High Magnetic Fields in Semiconductor Physics*, ed. by G. Landwehr, Springer, Berlin (1992), p. 56.
25. D. Shahar, M. Hilke, C. C. Li, D. C. Tsui, S. L. Sondhi, and M. Razeghi, *Sol. St. Commun.* **107**, 19 (1998); E-print archives, cond-mat/9706045.
26. D. H. Lee, Z. Wang, and S. Kivelson, *Phys. Rev. Lett.* **70**, 4130 (1993).
27. P. T. Coleridge and P. Zawadzki, *Sol. St. Comm.* **112**, 241 (1999).
28. A. M. M. Pruisken, B. Škorić, and M. A. Baranov, *Phys. Rev. B* **60**, 16838 (1999); E-print archives, cond-mat/9807241.
29. S. Luryi, in *High Magnetic Fields in Semiconductor Physics*, ed. by G. Landwehr, Springer, Berlin (1987).
30. A. L. Efros, *Phys. Rev. B* **45**, 11354 (1992).
31. N. R. Cooper and J. T. Chalker, *Phys. Rev. B* **48**, 4530 (1993).